Purely rotational coherence effect and time-resolved sub-Doppler spectroscopy of large molecules. II. Experimental

J. Spencer Baskin, Peter M. Felker,[a] and Ahmed H. Zewail
Arthur Amos Noyes Laboratory of Chemical Physics,[b] California Institute of Technology, Pasadena, California 91125

(Received 3 November 1986; accepted 24 November 1986)

In this paper we describe the results of picosecond fluorescence polarization (sub-Doppler) experiments designed to determine the role of purely rotational coherence in two jet-cooled molecules: *trans*-stilbene and anthracene. Observations of the manifestations of purely rotational coherence in *t*-stilbene are reported. The relationship of purely rotational coherence to molecular parameters (excited state rotational constants and transition dipole directions) is confirmed by comparison of our measurements with the results of the theory described in paper I [P. M. Felker and A. H. Zewail, J. Chem. Phys. **86**, 2460 (1987)]. The sum of rotational constants B' and C' of the *t*-stilbene S_1 electronic state is determined with a precision of better than 1 part in 700 ($B' + C' = 0.5132 \pm 0.0007$ GHz). The influence of molecular beam expansion conditions and fluorescence detection conditions on our measurements is also investigated and compared with the theroretical findings of paper I. Also measurements of time-resolved and polarization-analyzed fluorescence as a function of excess vibrational energy in the S_1 electronic states of both *t*-stilbene and anthracene are reported. We are able to distinguish the contribution of purely rotational coherence from the contributions of purely vibrational (or rovibrational) coherence to the evolution of fluorescence from the vibrationally excited molecule. The results are first analyzed on the basis of a model in which strict separability of vibrational and rotational motion is assumed. This provides a test of the extent of coupling of these motions and its influence on intramolecular vibrational energy redistribution (IVR).

I. INTRODUCTION

In the preceding paper,[1] the theory of purely rotational coherence in isolated molecules has been presented. The conditions for detecting this coherence in large molecules, using picosecond fluorescence polarization techniques, have been established. In this paper we describe the results of picosecond fluorescence polarization experiments which serve to test the predictions of this theory in two molecules: *trans*-stilbene and anthracene. The molecules were cooled by supersonic expansion in a molecular beam, and their polarization-analyzed fluorescence detected by single photon counting techniques. All measurements were performed under collisionless conditions.

As previously reported,[2,3] the manifestations of purely rotational coherence, in the form of polarization-dependent transients, are clearly seen in *t*-stilbene fluorescence for $S_1 - 0_0^0$ excitation. We give here a full account of our observations of these manifestations at the *t*-stilbene origin and verify their relationship to molecular parameters (excited state rotational constants and transition dipole directions) by comparison of experimental results and the theory of paper I.[1] From these sub-Doppler excited state measurements, the sum of rotational constants B' and C' of the *t*-stilbene S_1 electronic state is determined with a precision of better than 1 part in 700. The influence of molecular beam expansion conditions and fluorescence detection conditions on the measurements is also investigated, and compared with the theoretical findings of paper I.[1]

To understand and separate the roles of vibrational coherence and rotational coherence in large molecules, we have also undertaken measurements of time-resolved and polarization-analyzed fluorescence as a function of excess vibrational energy in the S_1 electronic states of both *t*-stilbene and anthracene. The vibrational structure of the $S_1 \leftarrow S_0$ electronic transitions of both molecules have been well characterized up to total vibrational energies of approximately 2000 cm^{-1} by previous studies.[4–9] Extensive investigations of vibrational coherence through time-resolved fluorescence measurements (without polarization analysis) on the picosecond time scale have been reported for both *t*-stilbene[10] and anthracene.[11] In the present experiments, polarization analysis permits us to distinguish the contribution of purely rotational coherence from the contributions of purely vibrational (or rovibrational) coherence to the evolution of fluorescence from the vibrationally excited molecule. The results are first analyzed on the basis of a model in which strict separability of vibrational and rotational motion is assumed. This provides a test of the extent of coupling of these motions and its influence on intramolecular vibrational energy redistribution (IVR).

The outline of the presentation is as follows. In Sec. II we describe the experimental apparatus and procedures. Results of polarized fluorescence measurements of jet-cooled *t*-stilbene and anthracene are presented in Sec. III. The stilbene results are divided under the headings *Purely rotational*

[a] Current address: Department of Chemistry, University of California, Los Angeles, CA 90024

[b] Contribution No. 7500. This work supported by a grant from the National Science Foundation (DMR 85-21191).

 0021-9606/87/052483-17$02.10

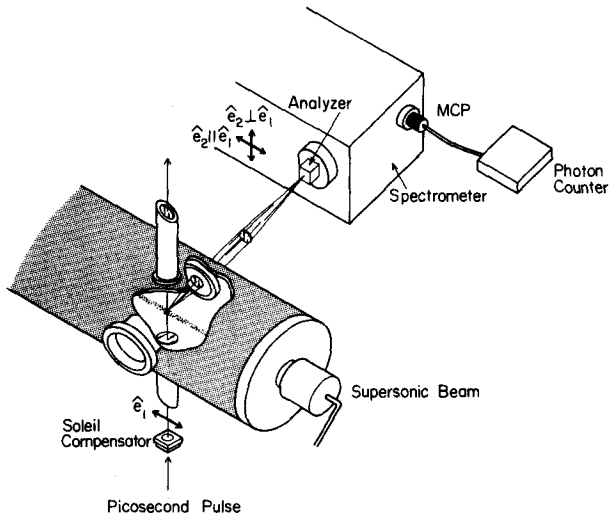

FIG. 1. Sketch of the experimental arrangement for the measurement of time-resolved and polarization-analyzed fluorescence of jet-cooled molecules. $\hat{e}_1$ is the polarization vector of the excitation pulse. $\hat{e}_2$ is the polarization component of the collected fluorescence that is selected by the prism analyzer for detection. Two possible orientations of $\hat{e}_2$ are shown. MCP is a microchannel plate photomultiplier. Pulse processing and timing electronics are incorporated in the "photon counter" black box.

coherence and *Excess vibrational energy dependence*. Section IV begins with a brief qualitative theoretical description of purely rotational coherence, summarizing those points essential to an appreciation of the discussion which follows. That discussion is subdivided in the same manner as Sec. III, and includes comparisons of our measurements with simulations based on the theory presented in paper I.[1]

II. EXPERIMENTAL

A. Molecular beam arrangements and expansions

Picosecond polarization experiments were carried out on jet-cooled samples of *trans*-stilbene and anthracene, obtained from commercial sources (Aldrich, Pfaltz, and Bauer) with stated purities $\geqslant 96\%$. Earlier work on these molecules carried out in this laboratory[4–7,10,11] has demonstrated that further purification has no effect on observed characteristics of the samples in the spectral region of interest.

The continuous supersonic jet apparatus consisted of a Pyrex sample reservoir and nozzle mounted horizontally within a translatable, heated metal jacket on the axis of a cylindrical vacuum chamber 12 in. in diameter (Fig. 1). An inert carrier gas was introduced into the reservoir via a simple double O-ring compression fitting to the back stem of the sample tube. The expansion of the seeded carrier gas occurred through a pinhole in the Pyrex nozzle. Unless otherwise noted, expriments were conducted using neon at a pressure of approximately 6 atm and a pinhole of diameter D ranging from 65 to 80 μ. The nozzle was maintained at a temperature approximately 50 °C higher than that of the reservoir to prevent clogging. An Edwards 18B4A 12 in. oil vapor booster pump, backed by a Kinney KT150 single stage mechanical pump, was connected to a right angle pneumatic valve mounted on the end of the 36 in. long chamber. With this arrangement, the background pressure was maintained below a few millitorr under all operating conditions of the molecular beam.

The expanding free jet was crossed by the vertically directed laser beam at a distance X from the nozzle, typically 2 or 3 mm. Pertinent expansion conditions, including X, D the reservoir temperature (T), carrier gas, and backing pressure will be cited when required in the next section as specific results are presented. In all these studies, careful checks for collisions (by studying the effect of changing X/D) were made.

B. Laser system

A spectra physics model 171 argon ion laser in modelocked operation was used to synchronously pump a tunable dye laser with cavity dumper. The dyes Rhodamine 590 and DCM provided coverage of the wavelenth range 597 to 722 nm needed for these experiments. Tuning was accomplished with a three-plate birefringent filter, alone or in combination with an ultrafine tuning étalon. The cavity dumper was operated at a repetition rate of 4 MHz, with output pulses in the 5 to 10 nJ range. These visible pulses were focused into an appropriately cut $LiIO_3$ crystal, angle tuned to generate phase-matched second harmonic pulses in the range 298 to 361 nm with typical conversion efficiencies of several percent. The bandwidth of the ultraviolet pulses was determined to be no greater than 5 cm^{-1} without and 2 cm^{-1} with the étalon in place, based on spectrometer scans of scattered laser light. Among those excitation energies for which data is presented, the étalon was used only at $S_1 + 1249$ cm^{-1} in *t*-stilbene and $S_1 + 1789$ cm^{-1} in anthracene. The narrower bandwidth was required at these energies to ensure adequate resolution of the desired excitation band.

C. Fluorescence detection

Fluorescence from the interaction region of the crossed molecular and laser beams was collected at right angles to both beams by a collimating lens and focused by a second lens onto the entrance slit of a microprocessor controlled 0.5 m spectrometer (see Fig. 1). At the exit slit, single photons were detected by a microchannel plate photomultiplier tube. The photomultiplier output pulses were amplified, discriminated, and used to trigger the start channel of a biased time to pulse height converter (TAC). The stop channel was supplied by the similarly processed output of a fast photodiode detecting the visible laser pulses. The TAC output was fed to a multichannel analyzer in pulse height analysis mode, producing the desired histogram of photon arrival times. After accumulation of a sufficient number of counts per channel, the data were transferred to a DEC PDP 11/23 computer for storage and analysis.

The time base for our measurements was calibrated by detecting visible dye laser pulses at the full 82 MHz repetition rate of the argon laser. The calibration was repeated several times during the course of experiments to evaluate the long term stability of the system. Biasing of photon detection to early times could be avoided by maintaining detection count rates below 10 kHz. In practice, saturation of the

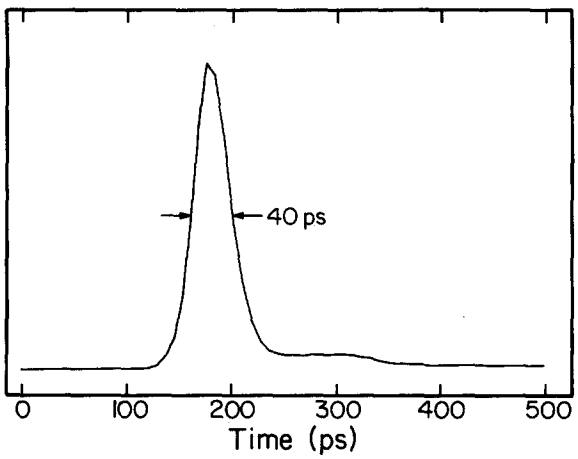

FIG. 2. Temporal response of the fluorescence detection system to scattered laser pulses. The spectral resolution is $\simeq 2\,\mathrm{cm}^{-1}$. A mask restricts the width of the spectrometer diffraction grating accessible to illumination. The long trailing edge is typical of the microchannel plate detector.

microchannel plate imposed a more stringent upper limit to detection rates of several kilohertz.

The temporal instrument response for the system was measured by advancing the tip of the nozzle into the laser beam and detecting the scattered laser light. In our efforts to minimize the response width, it was observed that the disparity in optical path lengths for different paths through the spectrometer could contribute significantly to the response time. For example, rays of 300 nm wavelength light which traverse opposite edges of our 76 800 groove grating have transit times differing by 77 ps in first spectral order. Therefore, during these experiments, a mask was placed immediately in front of the grating to reduce by more than two-thirds the width accessible to illumination. Figure 2 shows the optimum response of 40 ps FWHM obtained for the detection system described above, with the grating mask in place. Since the measured response was observed at times to be very sensitive to certain variables of the measurement procedure (spectrometer slit widths and grating position, and exact scattering geometry) and these factors were, in general, necessarily different for response and decay measurements, the measured response may be expected in some cases to differ from the one actually operative for the decay collection. Broadening due to long term instabilities is an additional impediment to precise determination of the effective response width for lengthy experiments. For accurate characterization of decays, we performed calibration experiments in which the response of the system was measured both before and after the transient measurement.

D. Polarization measurements

Our basic objective in these experiments was to separately detect components of fluorescence having polarizations oriented at selected angles with respect to the excitation polarization. The high degree of linear polarization required of the excitation source resulted naturally from the process by which the ultraviolet pulses were generated. A soleil compensator was used to orient the excitation polarization perpendicular to the direction of fluorescence collection. Analysis of the fluorescence into components was provided by a Glan-air prism placed before the entrance slit of the spectrometer (see Fig. 1). Since the acceptance angle of this prism construction (about 9 deg in the ultraviolet) surpassed that of the spectrometer, no unanalyzed light could reach the detector when the prism was correctly positioned. At some wavelengths this entailed biasing the prism normal slightly from the optical axis of the collection system in order to maintain a field of view symmetric about that axis.

The effect of the finite angle of fluorescence collection on mixing of polarization components was shown empirically to be minor by measuring decays with both our standard two lens $f2$ collection arrangement and a single lens arrangement of $f7$ with no apparent difference in results obtained. An indication of the polarization selectivity of the complete detection system was provided by measurements of scattered laser light. These tests showed the system adequate to provide a detection bias toward the selected polarization of no worse than 30 to 1.

An alternative but equivalent arrangement has also been employed for the detection of perpendicular fluorescence in which the compensator is removed, leaving the excitation polarization parallel to the direction of fluorescence collection. The prism analyzer is then unnecessary, and its removal results in a significant increase in signal at the detector.

E. Data treatment

We employed two principal techniques to quantify the differences observed in the temporal behavior of fluorescence decays acquired under conditions differing only in the setting of the polarization analyzer. The most generally applicable was the construction of the polarization anisotropy, defined as

$$r(t) \equiv \frac{I_{\parallel}(t) - I_{\perp}(t)}{I_{\parallel}(t) + 2I_{\perp}(t)},$$

where $I_{\parallel}(t)$ and $I_{\perp}(t)$ are the fluorescence intensities with polarizations parallel and perpendicular, respectively, to that of the excitation. The anisotropies presented have been calculated by the formula

$$R(t) \equiv \frac{[F_{\parallel}(t) - A] - a[F_{\perp}(t - t') - B]}{[F_{\parallel}(t) - A] + 2a[F_{\perp}(t - t') - B]},$$

where $F_{\parallel}(t)$ and $F_{\perp}(t)$ are the measured decays, A and B are their respective dark current imposed base lines, and a and t' are two adjustable parameters. Here the upper case R is employed (following the notation adopted by Negus *et al.*[12]) to emphasize that the effects of limited temporal response are directly incorporated into $R(t)$ and must be accounted for when comparing results with theory. The value of a was chosen to reproduce the theoretically expected[1] asymptotic value of the anisotropy, and t' was adjusted by consideration of the decay rises and very early behavior of $R(t)$. The need for these parameters arises from unavoidable changes in detection efficiency and time origin which are coincident with the change of detection polarization (i.e., the physical rotation of the analyzer).

Because $R(t)$ near $t = 0$ (taken as the instant that the decay amplitudes depart their base line values) is very sensi-

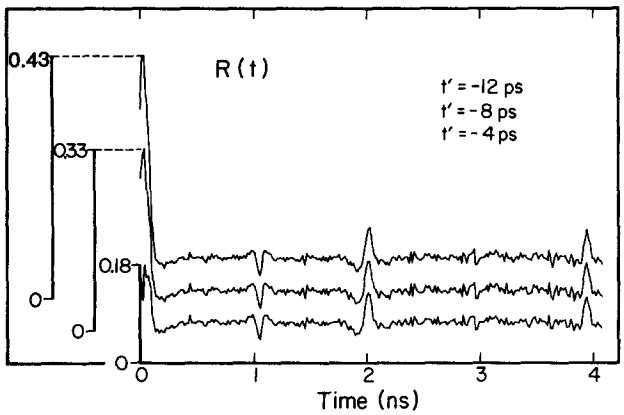

FIG. 3. Experimental fluorescence anisotropies $[R(t)]$ as a function of the temporal alignment parameter t' described in the text. Temporal resolution for the measured decays was 8 ps per data point. Fluorescence intensities at times intermediate to the measured data values are approximated by linear interpolation. $t = 0$ marks the position of the initial rise of fluorescence intensities above background level. The maximum value of $R(t)$ is indicated at left for each curve.

tive to small changes in t' as well as suffering from very low signal to noise, no attempt has been made to derive precise early time anisotropy values. In Fig. 3 is shown, for example, the effect of small variations in the value of t' on $R(0)$. Note, however that values of $R(t)$ at longer times are relatively insensitive to the choice of t', so that, in particular, the positions and amplitudes of recurrences, such as those observed in Fig. 3, are well determined. Similarly, apparent $R(0)$ values are strongly affected by even small response drifts, which again have negligible impact on $R(t)$ at other times.

A second technique of assessing the polarization dependence of our data was applied to certain decays measured at high excess vibrational energy whose temporal evolution was quasibiexponential in nature. In such cases, individual decays could be fit to a biexponential decay law using a nonlinear least squares fitting algorithm[13] and accounting for convolution with the measured response function. The behavior at early time of these decays is well characterized by the fast lifetime and fast-to-slow amplitude ratio obtained as parameters from such a fit. Measurements of fluorescence polarized parallel, perpendicular, and at 54.7° (magic angle) to the excitation polarization were compared on the basis of their respective fit parameters to determine the effect, if any, of polarization anisotropy transients on this early time evolution.

Extensive use was made of simulated data to evaluate the correspondence of experimental results and theoretical predictions. Numerical calculations of polarization-analyzed fluorescence intensities were made on the basis of the rotational coherence theory presented in paper I.[1] Details of the calculation procedure as applied to asymmetric top molecules are described in Sec. V B of paper I. A beat frequency resolution of 0.01 GHz and a temporal resolution of 8 ps were used for all simulations presented in this paper. The calculated intensities were convoluted with an appropriate measured system response to produce the simulated decays, which could then be analyzed by the methods described above. A thermally equilibrated, and hence isotropic, distribution of ground state molecules was always assumed. It was further assumed that the coherence width of the excitation source was sufficiently broad to span the entire rotational band contour of a vibronic transition. The choice of rotational constants, rotational temperature, and decay envelope (e.g., exponential or biexponential) used in the calculations will be considered in detail in the discussion.

III. RESULTS

A. *t*-Stilbene

1. Purely rotational coherence

In order to observe the manifestations of purely rotational coherence, free from the possibility of complicating vibrational effects, we carried out experiments exciting *t*-stilbene to its S_1 vibrationless level[4] at 32 234 cm^{-1}. Stilbene was a highly favorable choice for this purpose, due to its intermediate size, its geometry (near-symmetric top), and the direction of the transition dipole involved (approximately parallel to the long axis[14,15]). As will be seen, these factors lead to polarization anisotropies which are readily observable. Results are presented in Figs. 4 through 8, with experimental conditions given in the accompanying captions.

The results displayed in Figs. 4 through 7 were obtained detecting polarization-analyzed resonance fluorescence. The noteworthy feature of all these decays is the presence of periodic transients, or recurrences, which are detection polarization dependent. As can be seen in Fig. 4, these recurrences have opposite phase in the parallel and perpendicular decays while they are absent entirely for magic angle detection. This last fact indicates that the transients for parallel detection have twice the absolute amplitude of those for perpendicular detection (since $I_{54.7} \propto I_{\parallel} + 2I_{\perp}$, as discussed in paper I). For this reason, and to facilitate comparison, only parallel decays are shown in the following figures.

The persistence of polarization-dependent recurrences out to times of at least 14 ns (greater than five fluorescence lifetimes) is attested to by the decay of Fig. 5. Here also the

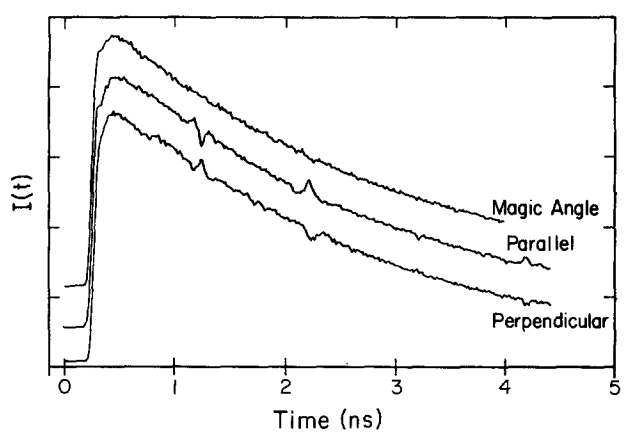

FIG. 4. Time-resolved and polarization-analyzed fluorescence for 0_0^0 excitation and detection of jet-cooled *t*-stilbene. The orientation of $\hat{e}_2$ relative to $\hat{e}_1$ is indicated for each decay. Detection bandwidth ($\Delta\bar{\nu}$): 12 cm^{-1}. Measured response: 40 ps FWHM. Supersonic beam conditions for these and following measurements (unless otherwise noted): 6 atm Ne, nozzle aperture diameter (D) $\simeq 65\ \mu$, laser to nozzle distance (X) = 3 mm, reservoir temperature (T) $\simeq 160$ °C.

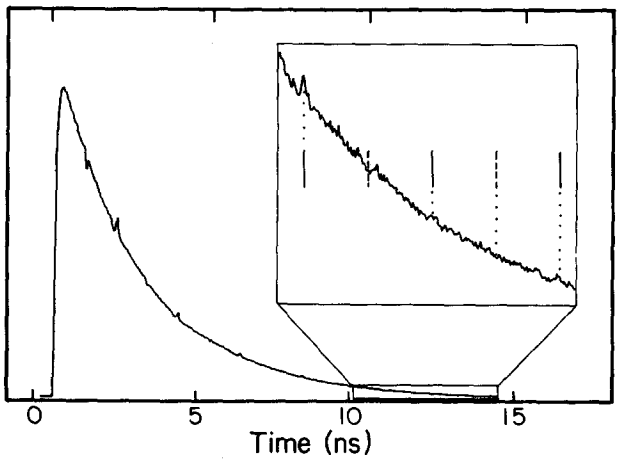

FIG. 5. Experimental polarization-analyzed fluorescence decay for 0_0^0 excitation and detection of jet-cooled *t*-stilbene. $\hat{e}_2$ is parallel to $\hat{e}_1$ in this and following figures when not explicitly indicated. The results of several separate experimental runs have been aligned and added together to produce this decay. Detection bandwidths: $< 4\,\mathrm{cm}^{-1}$. The last 4.5 ns of the data have been expanded in the inset with vertical solid and dashed lines indicating the positions at which in-phase and out-of-phase recurrences, respectively, are expected.

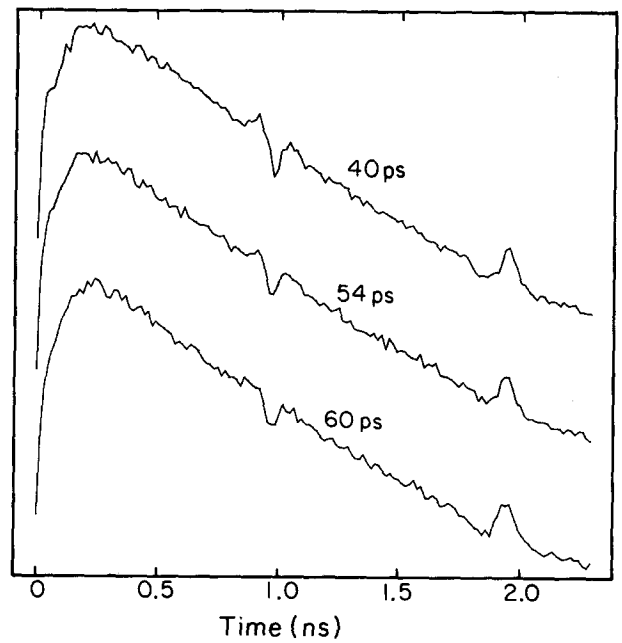

FIG. 7. Response width dependence of jet-cooled *t*-stilbene polarization-analyzed fluorescence decays. The value indicated is the average FWHM of the system responses measured before and after the decay. Conditions for all decays are as given in the caption of Fig. 4, except that $\Delta\tilde{\nu}$ for the bottom decay was $2\,\mathrm{cm}^{-1}$.

strict periodicity of the transients and their alternating pattern is clearly observed.

In Fig. 6 is shown an example of the influence of carrier gas pressure on our observations. Two and six atmospheres were the backing pressures employed for the top and bottom decays, respectively. The carrier gas was neon in both instances. All other conditions were identical. As the comparison reveals, the higher backing pressure produced a significant enhancement of the recurrence amplitudes. At a given pressure, the use of neon rather than helium as carrier gas also appeared to provide a noticeable though lesser enhancement of the recurrences. Based on these observations, 6 atm of neon was established as the standard expansion regime employed for the experiments described in this paper. Measurements at yet higher backing pressures of both neon and helium have been carried out (with the Pyrex sample tube replaced by one of metal), but the results have not differed substantially from those produced at 6 atm. (Examples of this will be seen in the decays of Fig. 9.)

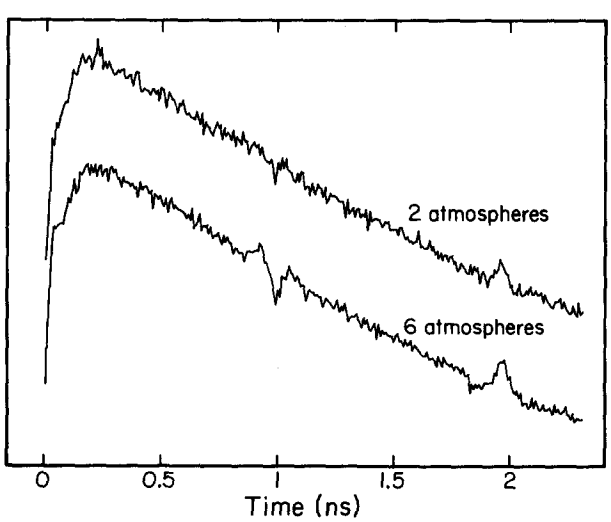

FIG. 6. Backing pressure dependence of jet-cooled *t*-stilbene polarization-analyzed fluorescence decays. The carrier gas is neon at the pressures indicated. All other conditions are as for Fig. 4.

Figure 7 offers a comparison of decays as a function of measured response width. The FWHM of the response functions associated with the decays shown are, from top to bottom: 40, 54, and 60 ps. The subtle differences displayed here are generally overshadowed by other influences such as variations in expansion conditions or response stability. These decays are, of course, themselves subject to the effects of the previously mentioned difficulties associated with response measurement. The influence which temporal resolution has on the appearance of recurrences in simulated decays will be examined in the discussion.

Figure 8 presents a selection of decays recorded once more for 0_0^0 excitation, but now detecting other than resonance fluorescence. The first and second decays result from detection of spectrally resolved emission bands at -204 and $-218\,\mathrm{cm}^{-1}$, respectively; for the third, spectral resolution is low and a number of bands contribute. Details of the detection conditions are given in the caption. In all cases the basic character of the polarization anisotropy remains unaltered from that displayed for resonance detection. Similar recurrences have also been seen in the region of totally unresolved fluorescence $10\,000\,\mathrm{cm}^{-1}$ below the excitation energy. There is at most a slight loss in recurrence amplitude in decays measured for detection of broadband fluorescence to distinguish them from spectrally resolved decays. Even this difference has not been conclusively established, in light of the many variables which may contribute to such an effect.

As has been shown in paper I[1] and will be discussed later, the period of recurrences due to rotational coherence is

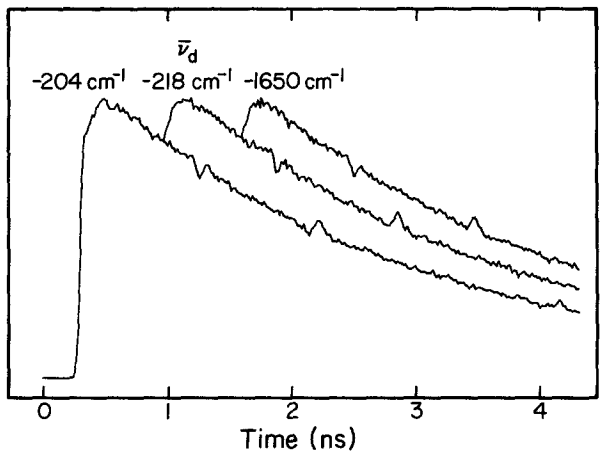

FIG. 8. Polarization-analyzed fluorescence decays for 0_0^0 excitation of jet-cooled *t*-stilbene. Shifts from the excitation energy of the centers of spectral detection ($\bar{\nu}_d$) are given in the figure. $\Delta\bar{\nu}$: (from left to right) 4, 3, 64 cm^{-1}. A single fluorescence collection lens was used for the -1650 cm^{-1} decay.

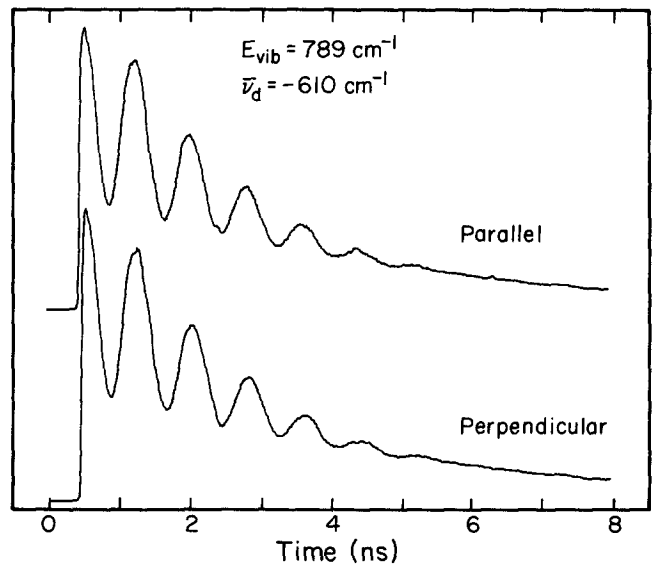

FIG. 10. Experimental polarization-analyzed fluorescence decays for $S_1 + 789$ cm^{-1} excitation of jet-cooled *t*-stilbene. $\bar{\nu}_d = -610$ cm^{-1}, $\Delta\bar{\nu} = 12$ cm^{-1}. Manifestations of both vibrational and rotational coherence are present.

determined by the geometry of the molecule in its excited state. Its precise value is thus of great interest. The period of full recurrence (i.e., the interval between transients of like phase) in the case of 0_0^0 excitation has been determined from the analysis of resonance fluorescence decays to be 1948.4 ± 2.5 ps. This same period, to within experimental error, is also measured for fluorescence collected at other detection wavelengths, such as those of Fig. 8.

The complete analysis, including a detailed comparison with theoretical predictions, of the above results and others to follow will be presented in the discussion section.

2. Excess vibrational energy dependence

The preceding experiments have clearly established the characteristics of purely rotational coherence in *t*-stilbene and the influence of experimental parameters on its observability. We now turn to an examination of rotational coherence in the vibrationally excited molecule. The time evolution of fluorescence in *t*-stilbene at excitation energies below $S_1 + 1300$ cm^{-1} has been extensively investigated in previous picosecond studies.[10] The manifestations of intramolecular vibrational energy redistribution (IVR) in the form of both periodic energy transfer (vibrational quantum beats), and dissipative redistribution are observed. Our objective in carrying out polarization-analyzed fluorescence measurements on these vibrationally evolving states is twofold: (i) to determine if the observed rotational coherence depends in any fashion on the excess vibrational energy, and (ii) to distinguish between the influence of rotational coherence and that of vibrational dynamics, for those cases in which both may contribute significantly to the time evolution of fluorescence. Results are presented below for excitations in each of the energy regimes classified by Felker *et al.*[10] on the basis of the type of IVR exhibited: no IVR (below 752 cm^{-1}), restricted IVR (789–1170 cm^{-1}), and dissipative IVR (above 1230 cm^{-1}).

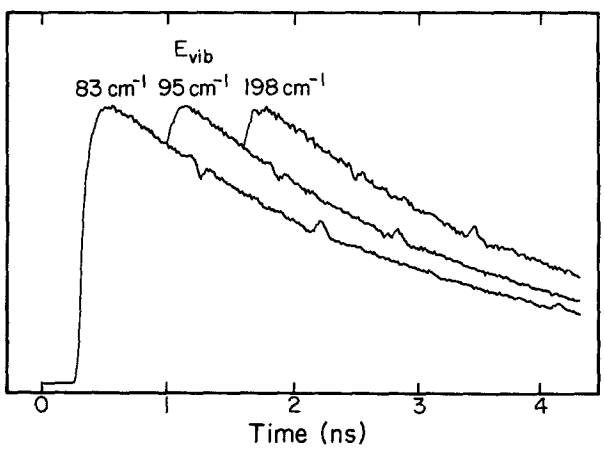

FIG. 9. Polarization-analyzed fluorescence decays of jet-cooled *t*-stilbene. Excitation energies above the S_1 origin are indicated. $\bar{\nu}_d$ and $\Delta\bar{\nu}$: (from left to right) -278 and 24 cm^{-1}, -260 and 9 cm^{-1}, -620 and 3 cm^{-1}. Approximate backing presures of helium: (from left to right) 38, 22, and 30 atm. For all three: $D = 25\,\mu$, $X = 1.5$ mm and $T \simeq 170$ °C.

Measurements at three different excitations in the low energy regime produced the three parallel decays of Fig. 9. These are virtually identical to those described in the previous subsection, with the familiar pattern of recurrences clearly in evidence. Variations in the decay rates may be discerned, but these are very slight (a few percent at most). Various detection wavelengths and bandwidths were employed for these measurements; again no apparent dependence on detection band is observed. Expansion conditions for these decays differed from the standard, as described in the caption. All measured recurrence periods have thus far remained within measurement uncertainties (~ 10 ps) of the origin (zero excess energy) value of 1948 ps. (The possibility of a slight change is suggested, however, by a measured recurrence period of 1942 ± 6 ps at 83 cm^{-1}. Further measurements are needed to establish this difference conclusively.)

Contrasting sharply with the low energy behavior are the results presented in Figs. 10 and 11, obtained for inter-

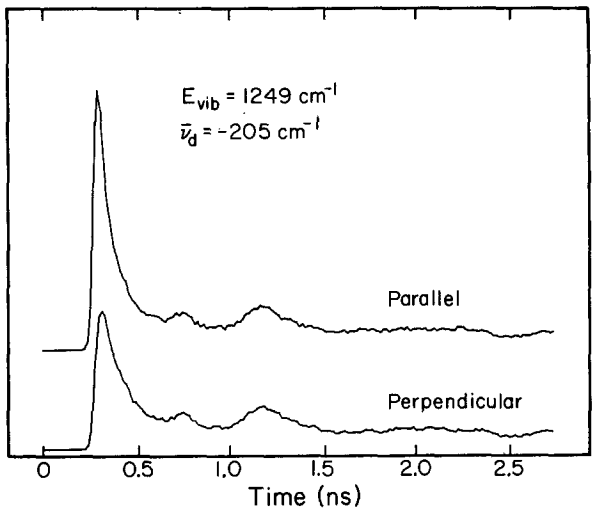

FIG. 11. Polarization-analyzed fluorescence decays for $S_1 + 1249\ \text{cm}^{-1}$ excitation of jet-cooled *t*-stilbene. $\bar{\nu}_d = -205\ \text{cm}^{-1}$, $\Delta\bar{\nu} = 32\ \text{cm}^{-1}$. The $-205\ \text{cm}^{-1}$ band is isolated and spectrally resolved at this bandwidth (Ref. 10).

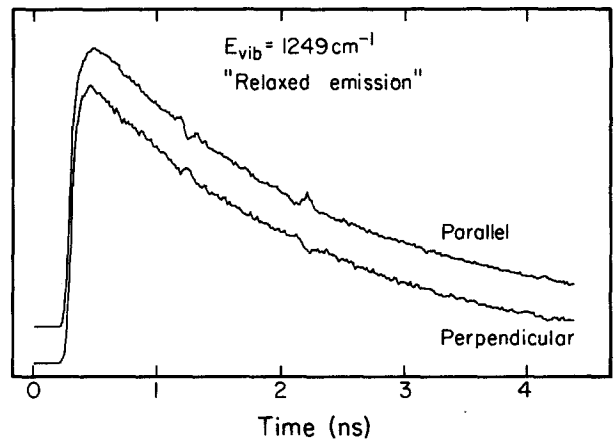

FIG. 12. Polarization-analyzed fluorescence decays for $S_1 + 1249\ \text{cm}^{-1}$ excitation of jet-cooled *t*-stilbene. $\bar{\nu}_d = -1640\ \text{cm}^{-1}$, $\Delta\bar{\nu} = 24\ \text{cm}^{-1}$. Fluorescence in this spectral region is totally unresolved (Ref. 10).

mediate (789 cm^{-1}) and high energy (1249 cm^{-1}) excitations, respectively. Parallel and perpendicular fluorescence for the same excitation and otherwise identical detection are compared in each figure. The spectrally resolved fluorescence band detected is in each case assignable as emission from the optically prepared superposition state.[4] The nature of the temporal evolution observed substantiates this assignment.[10]

The decays displayed in Fig. 10 for 789 cm^{-1} excitation are strongly dominated by a polarization-independent modulation. This modulation is attributable to a cyclic transfer of energy between two coupled zeroth-order vibrations (restricted IVR). In the presence of such strong modulations, the manifestations of rotational coherence may easily go unnoticed. Only at very high signal-to-noise may recurrences be seen, most prominently in the third trough and on the sixth peak of the vibrational oscillation. A framework permitting detailed comparison of these recurrences with those observed at the stilbene orgin will be developed in the discussion section.

In the decays of Fig. 11 (1249 cm^{-1} excitation) the influence of detection polarization is much more visible than in the preceding figure. Interestingly, the polarization anisotropy makes itself most evident here at a time—immediately after excitation—when none has heretofore been apparent. As we will show in the discussion, such an effect is expected as a consequence of the relation of our temporal response to the different time scales of evolution involved and is not necessarily an indication of a different mechanism at work. The very fast initial decay seen here represents the irreversible flow of vibrational energy out of the initially excited mode into the many equi-energetic bath modes of the molecule (dissipative IVR).[10] It is important to emphasize that detection for these decays was not at the laser wavelength and that careful checks were made to ensure that the observed fast components were completely free of scattered light.

In addition to the unrelaxed emission represented in Fig. 11, polarization-analyzed fluorescence in the vibrationally relaxed emission region for 1249 cm^{-1} excitation was also detected (Fig. 12). As for the preceding figures, both parallel and perpendicular fluorescence is shown. These decays resume the form observed for low energy excitations of a single exponential with the regular structure of polarization-dependent recurrences superimposed. That the recurrences appear less well defined in these decays than in others presented may be attributed solely to lower signal-to-noise. The measured recurrence period is unchanged (1943 ± 15 ps). The only discernible difference between the decays of Fig. 12 and those obtained at low energy excitation is their shorter lifetime. (2 ns vs 2.7 ns at low energies. A very short rise time may also be present but is unnoticeable here.)

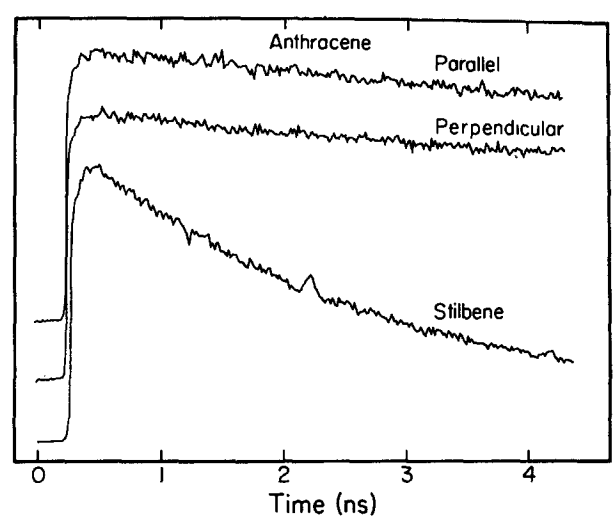

FIG. 13. Polarization-analyzed fluorescence decays for 0_0^0 excitation and detection of jet-cooled anthracene and *t*-stilbene. *T* for the anthracene decays was 175 °C, for the stilbene decay 155 °C. Other experimental parameters are listed for decays in order from top to bottom. $\Delta\bar{\nu}$: 24, 16, 4 cm^{-1}; *X*: 2, 3, 3 mm.

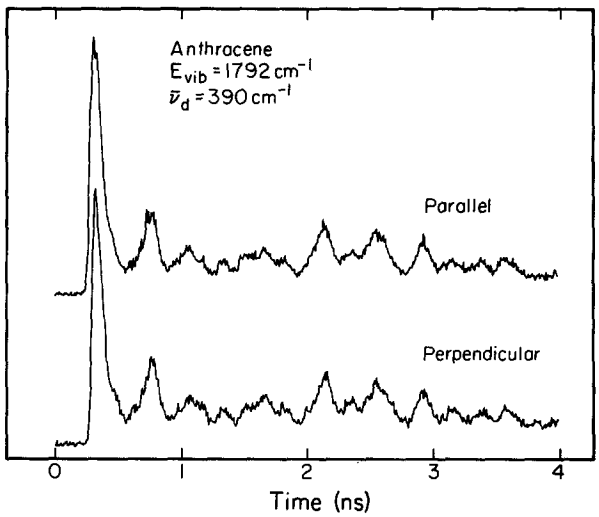

FIG. 14. Polarization-analyzed fluorescence decays for $S_1 + 1792\ \text{cm}^{-1}$ excitation of jet-cooled anthracene. $\bar{\nu}_d = -390\ \text{cm}^{-1}$, $\Delta\bar{\nu} = 160\ \text{cm}^{-1}$, $X = 2$ mm, $T = 175$ °C. The detected band is spectrally resolved at this bandwidth (Ref. 11).

B. Anthracene

Time-resolved fluorescence studies on the S_1–S_0 electronic transition of anthracene[11] have revealed each of the three quasidistinct categories of temporal evolution already described in reference to stilbene. Once again, each is found to occur at excitations within a particular range of excess vibrational energy in the S_1 state. To investigate the possibility of rotational coherence contributions to the observed fluorescence evolution, polarization-analyzed experiments analogous to, though less extensive than, those on stilbene were carried out on anthracene at excitations in these energy ranges.

The results for all excitation energies and detections studied may be quickly summarized as follows: Under conditions identical to those for which prominent polarization effects are seen in stilbene, anthracene fluorescence measurements show no distinct polarization dependence. Thus the influence of polarization anisotropy on fluorescence evolution in anthracene is considerably less than that observed in stilbene. The upper limit placed on this influence by our measurement uncertainties will be considered more carefully in the discussion. Examples of this effective polarization independence are displayed in Figs. 13 and 14. In Fig. 13 parallel and perpendicular decays of anthracene fluorescence for 0_0^0 excitation are compared with a comparable stilbene measurement. In Fig. 14 are shown data collected for high energy excitation ($1792\ \text{cm}^{-1}$). The fluorescence band detected to produce these decays is spectrally resolved despite the very wide detection bandwidth employed. Measurements under identical conditions, but in the absence of anthracene, confirmed that laser scatter gave no contribution to the observed fast component.

On the basis of these results, it may be concluded that rotational coherence has a negligible effect on the evolution of anthracene fluorescence as observed under experimental conditions similar to those employed here, regardless of the polarization properties of the light involved in excitation or detection. The evolution that is observed, such as the transients of Fig. 14 and other quantum coherence effects reported in Ref. 11, is therefore due exclusively to true intramolecular energy redistribution without contribution from the evolving ensemble-averaged orientation of the excited molecules that purely rotational coherence reflects. The degree to which the obvious disparity in the observed polarization dependence of anthracene and *t*-stilbene fluorescence is accounted for by the theoretical treatment of rotational coherence[1] will be examined in the following section.

IV. DISCUSSION

A. Rotational coherence in *t*-stilbene and anthracene

The detailed theoretical treatment of rotational coherence is given in paper I.[1] Here we give a brief description of the theoretical basis of the phenomenon, with emphasis on those aspects especially pertinent to our observations in *t*-stilbene and anthracene. In the experiments under discussion, multiple excited electronic state rotational levels are coherently prepared by laser excitation from a single ground state rotational level, as permitted by the appropriate electromagnetic transition selection rules and the laser bandwidth. Since these excited state levels may in turn emit to certain common ground state levels, quantum interference effects are expected in fluorescence when the detection does not resolve the separate emission channels.[16] In this case, the fluorescence will be modulated at frequencies corresponding to the energy splitting between the interfering excited state rotational levels, with amplitudes which depend on the particular excitation/emission channels involved. Since fluorescence polarization also varies with rotational state, the resultant beat pattern is detection polarization dependent.

For a rigid prolate symmetric top molecule, the rotational levels in the excited state have energies given by $E/h \equiv F(J',K') = B'J'(J'+1) + (A' - B')K'^2$ where A', B', and C' are the excited state rotational constants, and J' and K' are the quantum numbers for total angular momentum and projection of angular momentum along the symmetry axis, respectively. Selection rules are $\Delta J = 0, \pm 1, \Delta K = 0$ for parallel dipole transitions and $\Delta J = 0, \pm 1, \Delta K = \pm 1$ for perpendicular dipole transitions. Thus, for a given vibronic transition from a single ground state (J,K) level, three and six different excited state levels may be reached for parallel and perpendicular transitions, respectively. For parallel transitions the three resulting energy differences, and hence possible beat frequencies, are always multiples of $2B'$, whatever the initial (J,K) level. Five of the 15 differences between the six energy levels for perpendicular transition take on identical values, so at most ten distinct frequencies may be involved. Again, three are multiples of $2B'$, the fourth is a multiple of $4(A' - B')$, and the six others are $\nu_i \pm \nu_4$ where $i = 1$, 2, and 3, which are not, in general, multiples of any combination of molecular constants. The actual beat frequencies depend in both cases on the initial (J,K) level involved, so that the rotational beat patterns arising from different initial states will be different.

Since, in practice, even at the low rotational temperatures attainable in supersonic expansion, many ground state rotational levels are occupied, the fluorescence actually monitored in an experiment will be an incoherent superposition of many different beat patterns displaying a wide range of modulation frequencies. The individual modulations due to specific initial states will be lost in this averaging process. Those modulations having frequencies which share a common divisor, however, will periodically rephase at the frequency of the common divisor. Thus, even when individual beat patterns cannot be distinguished, the existence of commensurable frequencies in these patterns will lead to macroscopic recurrences in the fluorescence intensity as rephasing occurs. For parallel transitions this rephasing is complete—every frequency of every molecule is a multiple of $2B'$—and full recurrences are expected at times $n/2B'$, for $n = 1,2,\ldots$. Moreover, it is shown in paper I that in this case all modulation amplitudes have the same sign when either the parallel or the perpendicular polarization component of fluorescence is detected, so that beat components interfere constructively at these times. This is true whether the direction of the transition dipole in emission is parallel or perpendicular. When exciting perpendicular transitions, the number of beat frequencies actually involved depends on the emission dipole direction. However, it is a general result that not all components are of like sign. When all ten possible frequencies appear, which occurs for perpendicular transitions in emission, there will be partial recurrences only at times $t = n/2B'$ and $t = n/4(A' - B')$.

For slightly asymmetric tops (near-prolate), such as stilbene and anthracene, the rotational energy levels are given approximately by[17]

$$F(J',K') = \tfrac{1}{2}(B' + C')J'(J' + 1) + [A' - \tfrac{1}{2}(B' + C')]K'^2$$

for $K' = 0,1,\ldots,J'$. (To each $K' \neq 0$ will correspond two levels slightly split by asymmetry.) In addition, while selection rules on K are no longer strict, the symmetric top rules still apply qualitatively. Thus the preceding treatment of symmetric tops may be applied directly, to good approximation, to slightly asymmetric tops, with B' simply replaced by $1/2(B' + C')$. The usefulness of this treatment will, of course, diminish as the degree of asymmetry in the molecule increases.

B. Stilbene

1. Preliminary

Gas-phase electron diffraction studies[18] have yielded considerable information on the ground state geometry of isolated *t*-stilbene. The following ground state rotational constants have been calculated on the basis of these results: $A'' = 2.675\,\text{GHz}, B'' = 0.258\,\text{GHz}, C'' = 0.246\,\text{GHz}$. It has been assumed for the purpose of these calculations that the ethylene is planar and that the phenyl rings are rotated in opposite sense 30° out of plane, resulting in C_2 molecular symmetry. The values of these angles of rotation are considered particularly uncertain,[18] and many theoretical studies[19,20] have suggested a more nearly planar geometry. The uncertainties in these and other determined structural parameters lead to an uncertainty in the derived rotational constants of only about 2% however. Thus *t*-stilbene, in its ground electronic state at least, is only very slightly asymmetric ($|b| < 0.005$, where b is a commonly used measure of asymmetry defined by

$$b = \tfrac{1}{2}(C - B)/[A - \tfrac{1}{2}(B + C)]),$$

and the simplified symmetric top treatment of rotational coherence is expected to apply quite well. Furthermore, previous work[5,14,15] has established that all investigated $S_1 \leftarrow S_0$ vibronic transitions are best characterized as A axis polarized or parallel in the prolate symmetric top limit. Thus with appropriate excitation and detection, the fluorescence of stilbene, based on the preceding brief considerations, is expected to display polarization-dependent recurrences of period $1/(B' + C')$.

In order to verify that the recurrences we have observed do indeed arise by the process described above, a quantitative assessment of the amplitudes of rotational coherence beat components and of the effects of thermal averaging has been undertaken and will be compared with our experimental results below. Nevertheless, at this point we already have in hand a highly suggestive quantitative test of the identity of the observed recurrences. From the measured period of stilbene recurrences, and assuming the relation above, the sum of excited state rotational constants can be derived: $B' + C' = 0.5132 \pm 0.0007\,\text{GHz}$. Both rotational band contour analysis[5] and Franck–Condon analysis[4] have indicated significant differences in the geometry of stilbene in its S_0 and S_1 electronic states. A $(1 \pm 1/2)\%$ average increase in rotational constants was estimated in the former, while the latter estimated a change in the normal coordinate of the ν_{25} vibrational mode (approximately equal to the C=C–ϕ bend angle) that would in itself entail a change of 0.5% in both B and C constants. Theoretically calculated ground and excited state structures[19] indicate that the sense of the ν_{25} distortion upon excitation is such as to increase B and C. The total increase in $B + C$ predicted by these calculations is also about 1%. Based on these findings and the ground state data previously cited, a best estimate of $B' + C'$, independent of our rotational coherence measurements, would be $0.509 \pm 0.01\,\text{GHz}$. The success of this comparison alone can leave little doubt as to the nature of the phenomenon observed. As shown in Refs. 3 and 21, further confirmation is provided by measurements of $B' + C'$ for d_{12}-stilbene, and stilbene–Ar and stilbene–He complexes.

2. Purely rotational coherence

In Fig. 15 are displayed simulations of polarization-analyzed fluorescence decays for stilbene 0_0^0 excitation. (The simulation procedure is described in Sec. II.) The transition moments in both absorption and emission are taken to be parallel. A detection response of 50 ps FWHM, a rotational temperature (T_{ROT}) of 2 K, and rotational constants $A' = 2.675$ GHz, $B' = 0.273$ GHz, and $C' = 0.240$ GHz have been assumed. These parameters were chosen to reproduce closely measurements at our standard expansion conditions. The agreement of these decays with those experimentally observed at the *t*-stilbene origin (Fig. 4) is obviously

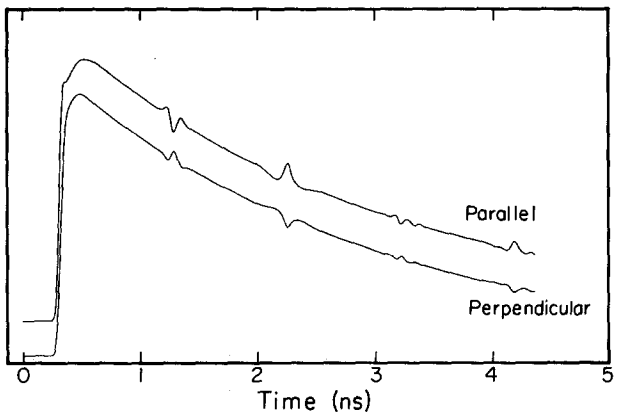

FIG. 15. Numerically simulated time-resolved and polarization-analyzed fluorescence accounting for purely rotational coherence. The following parameters were used in the rotational coherence calculation. Transition dipole moment directions: (‖,‖); ground state rotational temperature (T_{ROT}): 2 K; rotational constants: $A' = 2.675$ GHz, $C' = 0.240$ GHz, $B' = 0.273$ GHz. A single exponential population decay of lifetime 2.7 ns is assumed. The calculated intensity has been convoluted with a measured temporal system response of 50 ps FWHM.

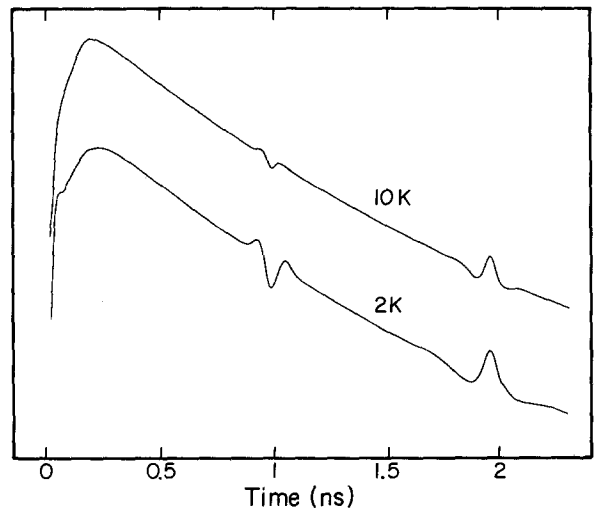

FIG. 16. Simulated time-resolved and polarization-analyzed fluorescence accounting for purely rotational coherence: temperature dependence. The value of T_{ROT} used in the calculations is indicated. All other parameters are as given in the caption of Fig. 15.

excellent. In the following paragraphs we examine the influence of adjustable parameters in these simulations, with a view to testing the reasonableness of the choices made above.

Attempting to reproduce the width, amplitude, and separation of observed recurrences by varying T_{ROT}, B', and C' (with other parameters fixed) led uniquely to the set of values used for the simulations of Fig. 15.[22] The temperature of 2 K obtained by this process is consistent with the temperature estimated for similar expansion conditions from stilbene rotational band contours.[5] As has already been pointed out, the sum $B' + C'$ may be determined very accurately by measurement of the recurrence period, and the value of 0.5132 GHz for *t*-stilbene was determined on that basis. In contrast, individual values for B' and C' were derived by considering the line shape of the recurrences, while holding their sum fixed at the previously determined value. The resulting values differ by about 4% from those obtained by a uniform adjustment of the calculated ground state constants (C_2 geometry), given earlier. However, this difference falls to less than 2% when either a planar geometry or C_i geometry for stilbene is assumed for the ground state calculation.[23] While further work is needed to test the accuracy of the separate B' and C' values indicated by these preliminary investigations, our experience to this point does indicate that the line shapes of rotational coherence recurrences exhibit significant sensitivity to changes in asymmetry. Thus the measurement of purely rotational coherence offers a promising means of determining not only those combinations of rotational constants fixed by the recurrence periods, but the values of individual constants as well.

For the simulations of Fig. 15, a rotational temperature of 2 K was assumed. In Fig. 16 an expanded view of the $T_{ROT} = 2$ K simulation is compared to one for which $T_{ROT} = 10$ K, all else remaining unchanged. The effect of increasing temperature is in good agreement with the trend in Fig. 6, in which lower backing pressure, which is known to provide less effective rotational cooling,[5] was seen to produce less prominent recurrences. This effect is easily understood within the framework of rotational coherence.[1] As higher ground state rotational levels are populated, more beat patterns with higher modulation frequencies contribute to the thermal average. The result is increasingly fast dephasing of the recurrences, as rigorously established in Sec. IV C 3 of paper I.[1] Convolution of these sharper recurrences with the detection response leads in turn to smaller apparent amplitudes, as observed here in both experiment and simulation.

In Fig. 17 the effect of varying temporal response width on the appearance of rotational coherence recurrences is dis-

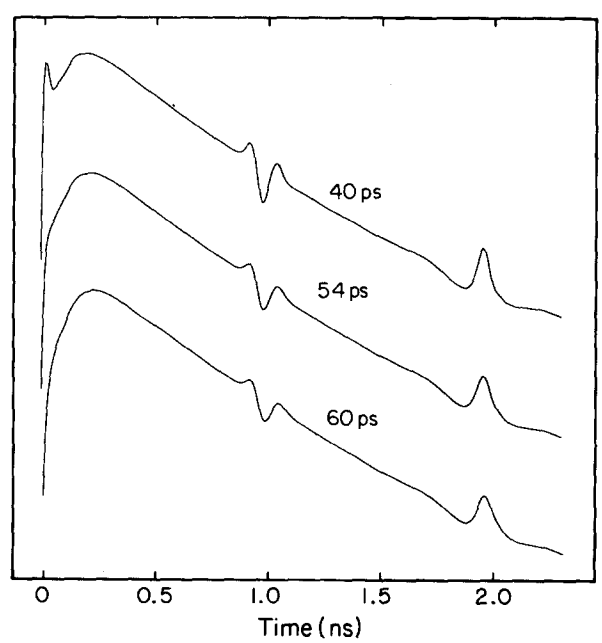

FIG. 17. Simulated time-resolved and polarization-analyzed fluorescence accounting for purely rotational coherence: response width dependence. The FWHM of the response used in the calculation of each decay is indicated. All other parameters are as given in the caption of Fig. 15.

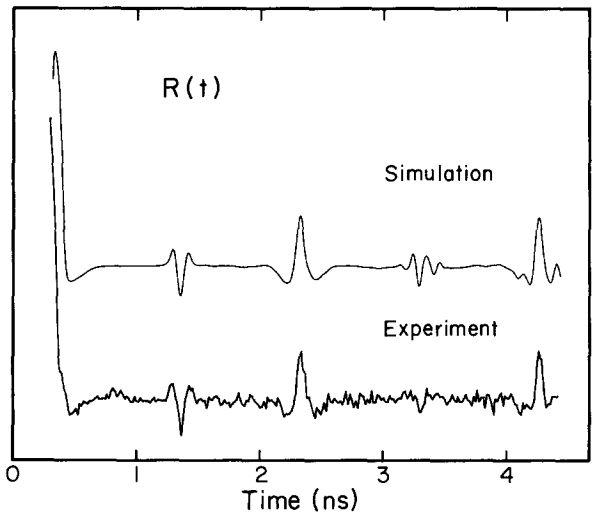

FIG. 18. Fluorescence polarization anisotropies formed from the decays of Fig. 4 (bottom) and Fig. 15 (top). The normalization of the experimental decays for the calculation of $R(t)$ for this and following figures was chosen to give a "residual" $R(t)$ value of 0.075.

played. These simulations should be compared against the measurements of Fig. 7. The slight broadening and damping of the recurrence as a function of increasing response width is comparable in the two figures. In the simulation using a 40 ps response there is a distinct spike in the fluorescence at early time. The early time anisotropy that this feature reveals will be discussed further below. Note, however, that this spike is absent in the corresponding measured decay of Fig. 7. On the other hand, simulations using a 50 ps response match the 40 ps measurements very well (cf. Figs. 15 and 4). This may simply indicate that the effective response in this case was broader than those measured. As previously mentioned, such a broadening is not unexpected when the duration of the decay measurement far exceeds that of the response measurement. Thus a difference between measured and effective response of the magnitude indicated here is quite reasonable.

Rotational coherence depends on the transition dipole direction but is otherwise independent of vibronic transition as long as the separation of rotational and vibronic wave functions is valid. This separation is assumed for all simulations presented in this paper and, in particular, dictates that simulations for all parallel transitions in the 0_0^0 dispersed fluorescence spectrum of *t*-stilbene would be identical to those of Fig. 15. That no detection wavelength dependence was seen experimentally is therefore consistent with (and lends strong support for) both separability of rotational and vibrational motion at the energies in question and the assignment of all detected bands as essentially parallel-type. (Note, however, that since the frequencies of rotational beat components are determined solely by the rotational energy levels in S_1, even if the rotational levels reached in S_0 were perturbed by vibrational motion, the *period* of recurrences would not be affected.)

For a more careful quantitative comparison of theory and experiment we present in Fig. 18 polarization anisotropies formed (as described in Sec. II E), from the data of Fig. 4 and the simulations of Fig. 15, respectively. Several noteworthy features of rotational coherence, which are not apparent upon examination of the decays themselves, may be readily observed in this figure. An example is the prominent early time anisotropy which is generally concealed in the rise of the fluorescence intensities. This anisotropy was clearly manifested in the measurements presented in Sec. III only in the high energy unrelaxed emission of Fig. 11. The top simulation of Fig. 17 indicates, however, that it could also be easily seen in the origin emission with a sufficiently fast and stable response. For a perfect symmetric top undergoing parallel transitions, our considerations have shown that the manifestations of rotational coherence are strictly periodic with period $1/2B'$. The full calculation[1] indicates that the true molecular anisotropy due to rotational coherence is equal to 0.4 at times $n/2B'$,$n = 0,1,2,\ldots$. The $R(t)$ values seen at early times in Fig. 18 are close to this value. That subsequent peaks are much smaller is due both to limited temporal response and asymmetry. Even when $r(t)$ is strictly periodic, returning to 0.4 at regular intervals, $R(t)$ away from $t = 0$ will not return to its initial value. This is a consequence of the discontinuity in the probability of emission (from 0 to its maximum value) at the instant of excitation. Asymmetry results in a further reduction of recurrence amplitudes [as reflected in the simulated $r(t)$'s in Fig. 7 of paper I, where no response function convolution is involved]. In Fig. 18 this damping is most evident for the out-of-phase recurrences and, as seen, is well accounted for by the simulation.

Also evident in Fig. 18 is the nonzero baseline value of $R(t)$. This residual anisotropy is expected also on purely classical grounds, since isolated molecules are constrained by energy and angular momentum conservation to a limited domain of spatial orientations. Thus memory of the initial alignment produced by the excitation process is never entirely lost. Since the time evolution of a rotating rigid body depends only on its moments of inertia and initial rotational state, the residual polarization anisotropy of fluorescence due to excitation from a thermal ground state population of molecules may depend only on T and the rotational constants.[25] Calculated values of the steady-state branch averaged fluorescence polarization of a symmetric top in the regular rotor limit are shown[25(a)] in Fig. 1 of Nathanson and McClelland as a function of the ratio of rotational constants. From our rotational coherence simulations for jet-cooled stilbene we find a residual anisotropy of 0.075. (An independent determination of this value was not made experimentally. See Sec. II E for details.) This value is very insensitive to the temperature and is identical to the value derived from Fig. 1 of Ref. 25(a) for a ratio of rotational constants of 10.4 corresponding to our assumed $A'/1/2(B' + C')$.

The preceding comparisons have firmly established the correspondence between our experimental observations and the theoretically predicted manifestations of purely rotational coherence.[1] The basic structure of the observed transients, their polarization dependence, temperature dependence, and relation to molecular geometry are all in full accord with theory. The applicability of rotational coherence theory at higher excitation energies will be examined next.

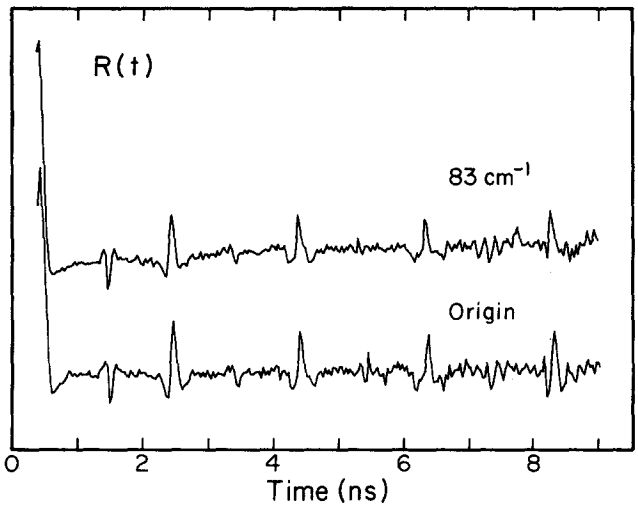

FIG. 19. Experimental fluorescence polarization anisotropies for 0_0^0 excitation (lower) and 83 cm^{-1} excitation (upper) of jet-cooled *t*-stilbene. For the origin measurement: $\bar{\nu}_d = 0\,cm^{-1}$, $\Delta\bar{\nu} = 2\,cm^{-1}$. Conditions for the 83 cm^{-1} measurement are as given for the leftmost decay of Fig. 9. Response widths were in each case 60 ps FWHM.

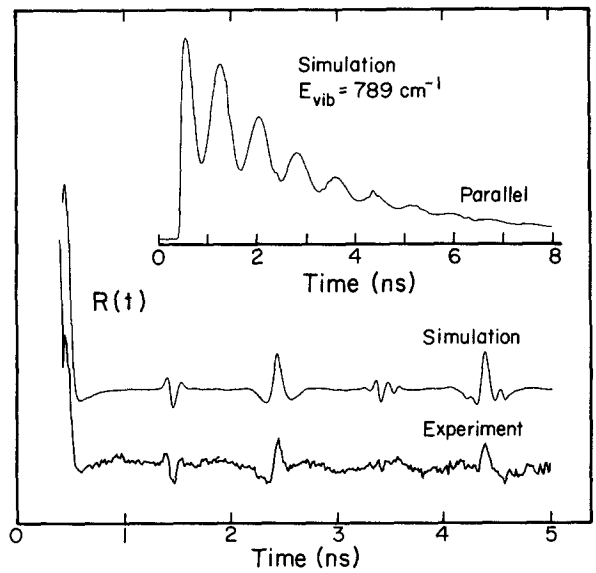

FIG. 20. Comparison of experimental and simulated fluorescence polarization anisotropies for $S_1 + 789\ cm^{-1}$ excitation of jet-cooled *t*-stilbene. The lower $R(t)$ was formed from the decays of Fig. 10; the upper from parallel and perpendicular fluorescence simulations, the first of which is shown in the figure. Simulation parameters for the calculation of purely rotational coherence $[C_\alpha(t)]$ are as given in the caption of Fig. 15. The assumed vibrational envelope is given by $V(t) = [1 + 0.6\exp(-t/2.9\ ns)\cos(2\pi t/0.79\ ns)]\exp(-t/2.7\ ns)$.

3. Excess vibrational energy dependence

As mentioned previously, when strict separation of rotational and vibrational motion is assumed, rotational coherence is independent of the vibrational levels reached either in absorption or emission. In this case, polarization-analyzed fluorescence, as shown in paper I,[1] evolves as the product of a polarization independent envelope reflecting vibronic evolution [which we shall call $V(t)$] and the purely rotational coherence function appropriate to the given detection polarization [$C_\alpha(t)$ where α identifies the direction of detection polarization]. Thus

$$I_\alpha(t) = V(t)C_\alpha(t).$$

In the following, experimental results will be compared with simulations which have been based on this approximation. The functions $C_\parallel(t)$ and $C_\perp(t)$ will remain the same throughout and are just the rotational coherence contributions to Fig. 15.

It follows immediately from the above expression that the molecular fluorescence anisotropy is independent of $V(t)$:

$$r(t) = \frac{I_\parallel(t) - I_\perp(t)}{I_\parallel(t) + 2I_\perp(t)} = \frac{C_\parallel(t) - C_\perp(t)}{C_\parallel(t) + 2C_\perp(t)}.$$

For comparison with the experimentally measured anisotropy, however, one must account for the detection response $S(t)$:

$$R(t) = \frac{\int_{-\infty}^{+\infty} I_\parallel(t')S(t-t')dt' - \int_{-\infty}^{+\infty} I_\perp(t')S(t-t')dt'}{\int_{-\infty}^{+\infty} I_\parallel(t')S(t-t')dt' + 2\int_{-\infty}^{+\infty} I_\perp(t')S(t-t')dt'}$$
$$= \frac{\int_{-\infty}^{+\infty} [C_\parallel(t') - C_\perp(t')]V(t')S(t-t')dt'}{\int_{-\infty}^{+\infty} [C_\parallel(t') + 2C_\perp(t')]V(t')S(t-t')dt'}. \quad (1)$$

Thus the vibronic component does not simply divide out and $R(t)$ will depend on the form of $V(t)$, even when, as we shall assume here, $r(t)$ does not. In practice, this dependence is very slight unless $V(t)$ shows significant variation on the time scale of $S(t)$. The possibility that differences in $R(t)$ may be traceable to differences in $V(t)$ only should be kept in mind, however. Simulated anisotropies will prove useful in separating such convolution effects from the effect of real variations in $r(t)$.

With $R(t)$, we now have an effective means to evaluate the contribution of rotational coherence to measured decays displaying complicated and diverse temporal evolution, such as those in Figs. 10 and 11. The procedure will be to calculate the experimental $R(t)$ from the data and compare this with $R(t)$ derived from Eq. (1) with an appropriate choice of $V(t)$.

a. Low energy excitation. Polarization-analyzed measurements for low energy excitations have shown no significant difference from those for 0_0^0 excitation (cf. Figs. 4 and 9). For a closer comparison of the data, we present in Fig. 19 anisotropies for 83 and 0 cm^{-1} excitation. The very close agreement of these traces is apparent. Thus rotational coherence is essentially unaffected by vibrational excitation in the low energy regime. The match of recurrence periods also imposes a limit on the changes in rotational constants which may result as a consequence of vibrational motion. In the description outlined above, low energy excitations are characterized by a single exponential $V(t)$ with about the same lifetime as the origin. For this case (and assuming no change in rotational constants) the simulations of Figs. 15 and 18 apply without modification. The agreement of experiment and the predictions of this treatment indicates that the assumptions made are well satisfied at the energies in question.

b. Intermediate energy. In the case of 789 cm^{-1} excitation and $-610\ cm^{-1}$ detection (Fig. 10), $V(t)$ can be very well approximated by: $V(t) \propto [1 + \alpha e^{-\gamma' t}\cos(\omega t)]e^{-\gamma t}$, with appropriate choices of α, γ', and γ. In Fig. 20 are pre-

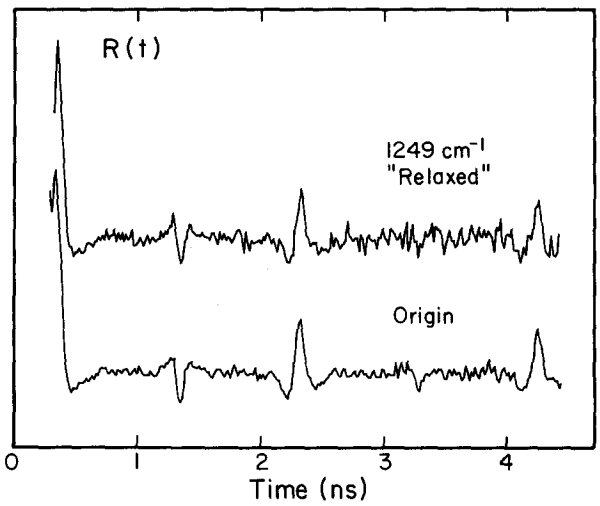

FIG. 21. Experimental fluorescence polarization anisotropies for 0_0^0 excitation (lower) and 1249 cm^{-1} excitation (upper) of jet-cooled *t*-stilbene. The lower trace is a more detailed view of the lower $R(t)$ of Fig. 19. The 1249 cm^{-1} $R(t)$ was formed from the decays of Fig. 12. Response widths were in each case $\simeq$60 ps FWHM.

sented a simulated parallel decay and simulated $R(t)$ using this $V(t)$, and the experimental $R(t)$ calculated from the 789 cm^{-1} decays of Fig. 10. In the experimental $R(t)$ of Fig. 20 the basic features seen in previous $R(t)$'s are again present. The recurrence period is also the same (1948 $\pm$ 15 ps). But there appears to be a new feature here, as well, in the presence of a weak periodic ondulation of the normally flat base line or residual value. This feature has been reproduced several times; we feel it is therefore unlikely that undetected changes in experimental conditions between parallel and perpendicular decay collection are responsible. In particular, a shift of the time origin does not account for this effect, as shown by variation of the parameter t' in the $R(t)$ calculation (see Sec. II). Since the period of the ondulation is, at least approximately, that of the vibrational envelope, another possible cause which must be considered is the convolution effect alluded to earlier. The considerable disparity between the vibrational period and the measured response width (790 ps vs 55 to 65 ps for the experiments in question)

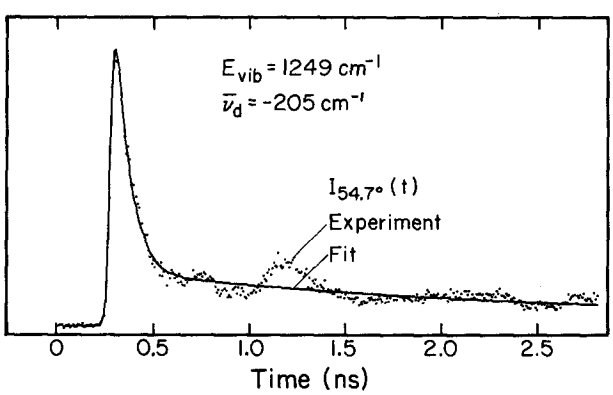

FIG. 22. Polarization-analyzed fluorescence decay for S_1 + 1249 cm^{-1} excitation: magic angle detection. $\bar{\nu}_d = -205\ cm^{-1}$, $\Delta\bar{\nu} = 32\ cm^{-1}$. The solid trace is the best fit biexponential accounting for convolution with a measured response of 55 ps FWHM.

precludes this as the source of any change in $R(t)$ as large as that observed. This is confirmed by the simulated $R(t)$ of Fig. 19 which shows no comparable influence of $V(t)$. Comparing this simulation with the simulation of Fig. 18 reveals that, in fact, in the given case $V(t)$ has absolutely no visible effect on $R(t)$ at all. Our results therefore indicate that there may be contributions to the fluorescence anisotropy other than those from purely rotational coherence. Such contributions could reflect a dependence of rotational motion on vibrational motion through, for example, centrifugal distortion (leading to a dependence of rotational constants on vibrational state) or Coriolis coupling.

c. High energy. For 1249 cm^{-1} excitation two different forms of decay were observed. For relaxed emission $V(t)$ is again single exponential. Though the lifetime is somewhat shorter than at the origin, this difference will have negligible effect on $R(t)$ due to the vastly different time scale of $S(t)$. This fact is amply confirmed by the agreement of the traces of Fig. 21, representing $R(t)$ at the origin and $R(t)$ constructed from the decays of Fig. 12. Once again, an absence of significant vibrational influence on $B' + C'$ is revealed by the measured recurrence period of 1943 $\pm$ 13 ps.

The $V(t)$ which corresponds to the unrelaxed emission of Fig. 11 is, on the other hand, a highly complicated function. A direct measurement of this function, subject to the limitation of our response, may be carried out by detection of magic angle fluorescence. [This is possible since $C_{54.7°}(t)$ is simply a constant.] In Fig. 22 is presented the result of such a measurement. The structure is roughly biexponential, with irregular partial recurrences at long times, as observed before.[10] Since it must in general be true that $I_{54.7°}(t) \propto I_{\parallel}(t) + 2I_{\perp}(t)$, $V(t)$ may also be obtained from a complete knowledge of $I_{\parallel}(t)$ and $I_{\perp}(t)$, including their relative intensities. This relation is valid under our experimental conditions regardless of the source of observed anisotropy. In practice this has been used to check the self-consistency of our data, which depends upon the theoretically determined normalization of parallel and perpendicular decays and the maintenance of uniform exprimental conditions throughout a series of polarization-analyzed measurements.

In order to simulate decays for comparison with those of Fig. 11 we shall adopt as a simple though useful approximation a biexponential $V(t)$. Approximate parameters for the description of $V(t)$ in this approximation were determined by biexponential fits of magic angle decays. An example is plotted against the data of Fig. 22. The fit is seen to reproduce the early time behavior very satisfactorily. For $V(t)$ given by

$$V(t) \propto f e^{-t/\tau_1} + e^{-t/\tau_2}$$

the parameters obtained are $\tau_1 = 44$ ps, $\tau_2 = 2.1$ ns, and $f = 10$ with uncertainties of about 10%. A biexponential fit of $I_{\parallel}(t) + 2I_{\perp}(t)$ formed from the decays of Fig. 11 yields parameters in good agreement with these. It must be noted that these parameters are quite sensitive to the response used in the fitting procedure; the large relative uncertainties directly reflect the uncertainty in the response.

With the parameters for $V(t)$ in hand, the simulations of Fig. 23 are readily calculated. A single measured response

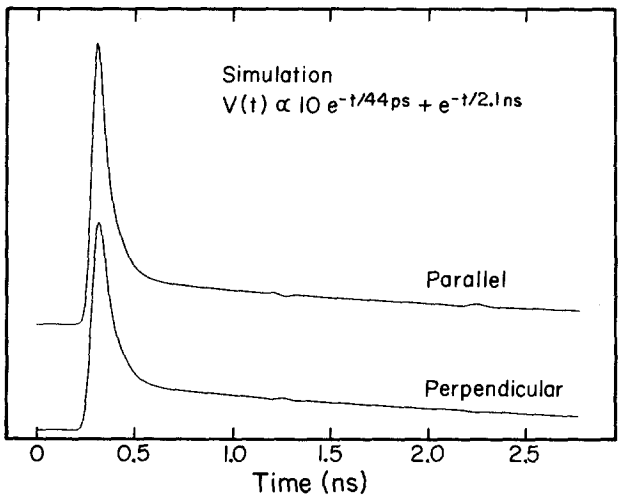

FIG. 23. Simulated time-resolved and polarization-analyzed fluorescence accounting for purely rotational coherence. Parameters for $C_\alpha(t)$ are as for Fig. 15. $V(t)$ is given in the figure. Calculated intensities are convoluted with a 55 ps response.

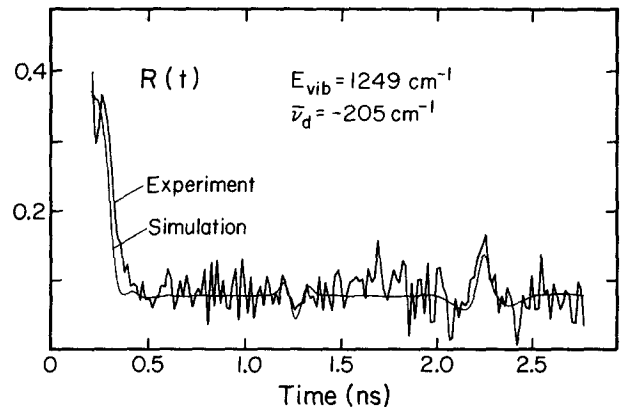

FIG. 24. Comparison of experimental and simulated fluorescence polarization anisotropies for $S_1 + 1249\ \text{cm}^{-1}$ excitation of jet-cooled *t*-stilbene. The experimental $R(t)$ was formed from the decays of Fig. 11; the simulated $R(t)$ from those of Fig. 23.

(55 ps FWHM) has been used in these simulations and in fitting all biexponential decays. One sees that rotational coherence does significantly influence the amplitude of the initial fluorescence spike, producing a polarization dependence similar to, though less pronounced that that displayed in Fig. 11. The quantitative agreement with experiment can be tested by comparison of parameters obtained from biexponential fits of corresponding sets of data. The results are given in Table I. In addition to fit parameters for the simulations of Fig. 23, for which the assumed rotational temperature was 2 K, parameters are also given for simulations assuming a temperature of $\frac{1}{2}$ K.

It is seen from these values that rotational temperature strongly affects the apparent decay parameters and that $T_{\text{ROT}} = \frac{1}{2}$ K gives much better agreement with the measured parameters than $T_{\text{ROT}} = 2$ K. This despite the fact that our measurements of recurrences for 0_0^0 excitation point strongly to the higher temperature. (Simulations using $T_{\text{ROT}} = \frac{1}{2}$ K predict much more prominent recurrences than those thus far observed.) A number of possible reasons for this discrepancy may be advanced. At the end of this section we note several points which may affect the accuracy of the purely rotational coherence calculations themselves. In the case of the observations at high energies, additional elements come into play. We have already seen evidence at intermediate vibrational energies suggesting a breakdown of the assumed separability of vibrational and rotational motion. At higher energies this is even more likely to occur, and could quite reasonably influence the results. Another factor to bear in mind is the assumed form of $V(t)$. Use of a more realistic model for the vibrational envelope may substantially alter the form of the simulated decays. Further work is needed to clarify the role of these factors.

TABLE I. Biexponential fit parameters for measured and simulated decays of *t*-stilbene $S_1 + 1249\ \text{cm}^{-1}$ unrelaxed fluorescence.

Detection polarization		Measured	Simulated 2 K	Simulated ½ K
$\hat{e}_2 \| \hat{e}_1$	τ_1(ps)	33	37	33
	τ_2(ns)	2.1	2.1	2.1
	f	17	13	16
$\hat{e}_2 \perp \hat{e}_1$	τ_1(ps)	56	47	53
	τ_2(ns)	2.2	2.1	2.1
	f	7.0	8.7	7.3

It is clear from the differences between parameters describing parallel, perpendicular, and magic angle data that the evolution of fluorescence may be significantly affected by rotational coherence. This fact should be borne in mind in the design and interpretation of time-resolved fluorescence experiments. In particular, in the study of vibrational dynamics, where $V(t)$ is sought, detection of other than magic angle fluorescence has the potential, at least, to be misleading. As we have seen, however, the degree of influence will depend not only on the particular molecule and excitation and detection arrangement, but also on the sample temperature. Thus previously reported parameters for $V(t)$ of the emission band currently under discussion[10] differ from those reported here due to the fact that perpendicular fluorescence was detected. They also differ from the experimental perpendicular detection parameters in Table I due to the lower rotational temperature obtained under the expansion conditions employed in the present study.

In addition to the highly visible anisotropy of the initial fluorescence spike, does unrelaxed emission display rotational coherence recurrences as well? The answer to this question is provided by the calculation of $R(t)$ from the decays of Fig. 11. This is shown in Fig. 24, along with $R(t)$ derived from the simulations of Fig. 23. Despite the low signal-to-noise of the experimental data, the recurrences are clearly observed. The measured period is 1932 ± 21 ps, still not conclusively different from the origin value. Note that the recurrence amplitudes and widths of the experimental $R(t)$ match quite well those of the simulation.

Careful examination of the simulated $R(t)$ of Fig. 24 at early time reveals certain irregularities not seen in the simulations of Fig. 18 or Fig. 20. This is further highlighted in Fig

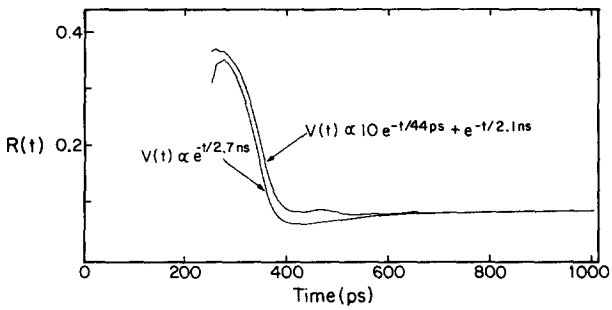

FIG. 25. Simulated fluorescence polarization anisotropies showing the dependence on $V(t)$. The upper trace is an expanded view of the simulated $R(t)$ of Fig. 24. $V(t)$ used in the calculation of each $R(t)$ is indicated. Other aspects of the two calculations were identical.

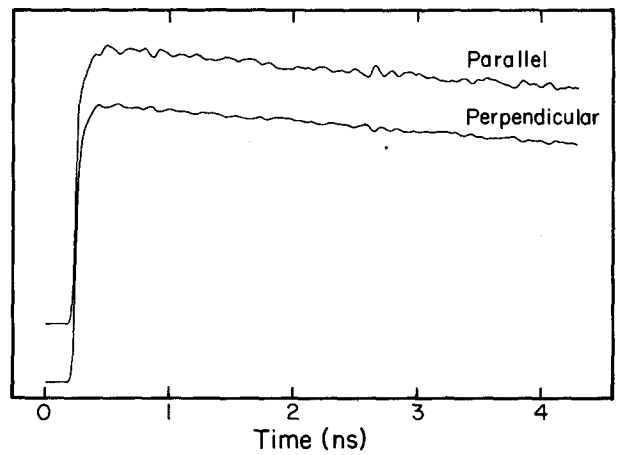

FIG. 26. Simulated time-resolved and polarization-analyzed fluorescence accounting for purely rotational coherence. Parameters for the calculation of $C_\alpha(t)$ are: transition dipole moment directions: $(\perp_B, \perp_B)$; ground state rotational temperature (T_{ROT}): 2 K; rotational constants: $A' = 2.134$ GHz, $B' = 0.446$ GHz, $C' = 0.371$ GHz. $V(t)$ is a single exponential ($\tau = 21$ ns). Calculated intensities are convoluted with a 53 ps response.

25. The upper trace is an expanded view of the simulation of Fig. 24, calculated using Eq. (1) and the $V(t)$ appropriate to 1249 cm^{-1} unrelaxed emission. The lower trace resulted from an identical calculation, changing only the form of $V(t)$. We see from this comparison that the biexponential $V(t)$ evolves sufficiently fast to exercise a small but distinct influence over the form of $R(t)$.

While only minor disagreement of simulation and experiment has been encountered in the foregoing, for the sake of completeness we wish to point out certain simplifying assumptions made in the course of the calculations which may not reflect exactly the experimental reality. In the case of *t*-stilbene, an important assumption underlying our calculations of purely rotational coherence which need not be strictly valid, either in absorption or emission, is that of a parallel transition dipole. Since stilbene has no symmetry axis in the *AB* plane and a distortion of the molecule on excitation is indicated, the possibility exists that the transition moment forms some small though unknown angle with the *A* axis. We have additionally found it convenient to restrict the transitions included in the calculations to those which are allowed by the selection rules on rotational subgroup species which are imposed in molecules of higher symmetry (D_{2h}) than *t*-stilbene. This greatly reduces the computation time, and the subset of transitions retained is a representative one. Another factor which has thus far been ignored is the influence of a limited coherence width in excitation. The calculated intensities apply strictly only when the coherence width of the laser is much greater than the rotational width of the vibronic transition in question. Caution on this point is thus particularly advisable in regard to the high energy measurements in *t*-stilbene (as also to those in anthracene, which will be considered below), in which the excitation bandwidth of one to two wave numbers was comparable to the width expected for rotational band contours at the temperature of our molecular beam.[5,7] The use of a single detection response to account for temporal spreads in both excitation and detection, and the assumption of a thermal, isotropic distribution of molecules following supersonic expansion, may also be sources of minor discrepancies between simulation and experiment. The influence of these and other factors should be kept in mind in the quest for a detailed understanding of vibrational and rotational coherence in *t*-stilbene, and large molecules in general.

C. Anthracene

In light of the sometimes very prominent display of rotational coherence in our stilbene measurements, the absence of comparable behavior in anthracene may seem surprising. As we have seen, the observable characteristics of rotational coherence are determined by the transition dipole directions in the molecule, its rotational constants, and the ground state rotational temperature.[1] From structural data on anthracene the following S_0 rotational constants have been calculated: $A'' = 2.154$ GHz, $B'' = 0.453$ GHz, and $C'' = 0.374$ GHz. Rotational band contour analysis, allowing for a single scaling factor between ground and excited state constants,[7] deduced a 1% reduction of the rotational constants in S_1 from the above values. Two differences between these values and those for stilbene have a significant bearing on the expected nature of rotational coherence. First, the asymmetry of anthracene is considerably more pronounced than that of stilbene ($b \simeq -0.02$ vs -0.003). This has the following effects: (i) The applicability of symmetric top selection rules is reduced, so that the number of interfering channels significantly involved in the fluorescence increases; and (ii) the energy levels are more strongly perturbed from the regular symmetric top spacing. Both of these effects diminish the commensurability of beat frequencies which is the source of macroscopic recurrences.[1] Second, the anthracene constants are larger than those of stilbene (reflecting its more compact structure). The modulation frequencies of individual beat components are thus proportionately higher as well, entailing faster dephasing of recurrences. (The increase in ground state constants will result in fewer initial levels being populated, but higher frequencies will still be involved, despite the lower J's.)

Also greatly affecting the form taken by rotational coherence are the directions of the dipole moments for the transitions involved, both in absorption and emission. The relative amplitudes of beat components are highly dependent on these. In anthracene the $S_1 \rightarrow S_0$ transition is *B*-axis

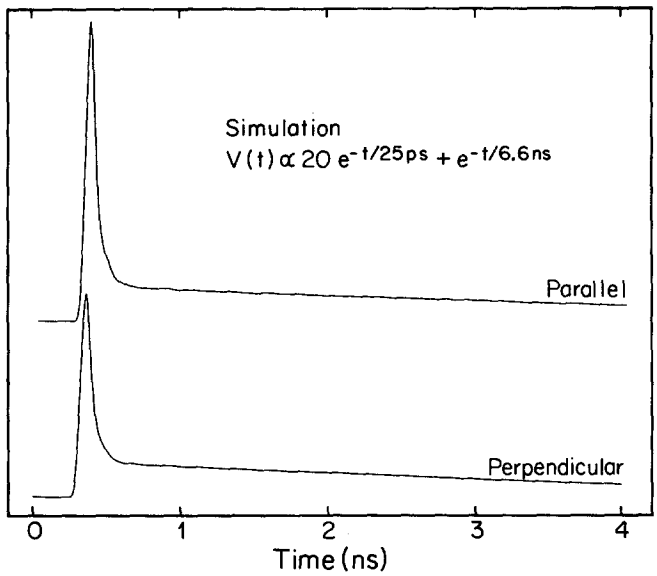

FIG. 27. Simulated time-resolved and polarization-analyzed fluorescence accounting for purely rotational coherence. Parameters for $C_\alpha(t)$ are as for Fig. 26. $V(t)$ is given in the figure, and approximates the decays of Fig. 14 for 1789 cm^{-1} excitation of anthracene. Calculated intensities are convoluted with a 57 ps response.

polarized, thus constituting a perpendicular transition in the symmmetric top limit. In this case, even for a symmetric top, many additional high frequency beat components are possible. In particular, it is shown in paper I[1] that, when the emission dipole is perpendicular as well, full recurrences are not expected and initial dephasing occurs on a much shorter time scale.

From the above considerations, the absence of obvious rotational coherence effects in anthracene on our current time scale is quite plausible. For a more rigorous test of the theory against our experimental results, we have produced simulated fluorescence decays for the $(\perp_B,\perp_B)$ case of purely rotational coherence.[1] These are displayed in Figs. 26 and 27. A rotational temperature of 2 K and rotational constants 1% lower than those cited above for the anthracene ground state were used for each simulation.

In Fig. 26 are presented parallel and perpendicular decays assuming a single exponential $V(t)$ with the lifetime of anthracene 0_0^0 fluorescence. The calculated intensities were convoluted with a response of 53 ps FWHM, corresponding to those measured in connection with the decays of Fig. 13. Some structure in the simulated fluorescence is seen, but, as expected, it is much less prominent than that in the case of stilbene. The recurrence periods in these simulations are $\tau_1 \equiv 1/(B'+C') = 1.224$ ns and $\tau_2 \equiv 1/4[A - 1/2(B'+C')] = 0.145$ ns. Thus the time scale of Fig. 26 covers many periods. Moreover, the most prominent recurrence seen in Fig. 25 (at ~2.7 ns on the plotted time axis) represents an accidental near coincidence of these two periods; i.e., $2\tau_1 \simeq 17\tau_2$. Small changes in the rotational constants will strongly affect such features, so that they cannot be well predicted if the constants are not precisely known. All other modulation amplitudes seen in these simulations fall well within the noise of the measurements of Fig. 13; thus experiment and theory as applied to anthracene 0_0^0 fluorescence are completely consistent.

The simulations of Fig. 27 were calculated using a biexponential $V(t)$ and parameters appropriate to the measured decays of Fig. 14 (1792 cm^{-1} excitation). In this case, the early time behavior deviates noticeably from that observed experimentally. Based on the measurements reported here, the possibility of a difference between polarization components of the magnitude displayed in Fig. 26 may be conclusively rejected. Comments made in regard to the deviation of measurement and simulation for the high energy measurements in *t*-stilbene are also appropriate here. To more fully characterize these systems, we plan future experiments with improved time resolution.

It should also be noted that certain bands in the anthracene excitation spectrum gain their strength through vibronic coupling[7] to a low-lying B_{3u} excited electronic state. The dipole moment is then parallel to the near symmetry axis as in stilbene, and the manifestations of purely rotational coherence are expected to change accordingly. Investigation of these bands is planned.

V. CONCLUSIONS

In this paper we have reported picosecond time-resolved, polarization-analyzed fluorescence measurements on jet-cooled *t*-stilbene and anthracene. The manifestations of purely rotational coherence in *t*-stilbene have been observed and thoroughly characterized via this measurement technique. An indication of the diversity of form which purely rotational coherence may exhibit in different molecular systems is provided by our observations in anthracene, in which no polarization-dependent behavior was observed. The results presented here agree well with the theoretical findings of paper I.

The usefulness of time domain fluorescence polarization measurement as a sub-Doppler spectroscopic tool has been demonstrated by the determination of molecular parameters (rotational constants and direction of the transition dipole) of *t*-stilbene in its first excited electronic state. This sub-Doppler feature of the technique is due to the fact that purely rotational coherence is an excited state beating phenomenon, which, as in quantum beats,[16] is Doppler free. Measurements of polarization anisotropies of fluorescence from excited vibrational levels in the *t*-stilbene and anthracene S_1 electronic states have permitted the separation of purely rotational coherence effects from purely vibrational coherence and other contributions to fluorescence evolution in the three regions of IVR (absent, restricted, and dissipative). Finally, observation of rotational coherences (recurrences) in stilbene up to 1249 cm^{-1}, which are similar to coherences at zero excess energy, indicates that the molecule is a well-behaved rotor at least up these energies.

Note added in proof: Recently, rotational coherence effects have also been observed with higher temporal resolution using pump–probe MPI in a molecular beam [N. Scherer, L. Khundkar, T. Rose and A. H. Zewail (to be published)]. The fluorescence technique has also been applied to the study of the retention of coherence in photodissociation processes (Ref. 21). Finally, rotational coherence

effects in four-wave mixing have been addressed by Hochstrasser's group [A. B. Myers and R. M. Hochstrasser, J. Chem. Phys. **85**, 6301 (1986)] in relation to studies (see paper I) of hot stilbene vapor.

ACKNOWLEDGMENT

We wish to thank David Semmes for helpful discussions and contributions to the experiments reported herein.

[1]P. M. Felker and A. H. Zewail, J. Chem. Phys. **86**, 2460 (1987).
[2]P. M. Felker, J. S. Baskin, and A. H. Zewail, J. Phys. Chem. **90**, 724 (1986).
[3]J. S. Baskin, P. M. Felker, and A. H. Zewail, J. Chem. Phys. **84**, 4708 (1986).
[4]J. A. Syage, W. R. Lambert, P. M. Felker, A. H. Zewail, and R. M. Hochstrasser, Chem. Phys. Lett. **88**, 266 (1982); J. A. Syage, P. M. Felker, and A. H. Zewail, J. Chem. Phys. **81**, 4685 (1984).
[5]B. W. Keelan and A. H. Zewail, J. Phys. Chem. **89**, 4939 (1985).
[6]W. R. Lambert, P. M. Felker, J. A. Syage, and A. H. Zewail, J. Chem. Phys. **81**, 2195 (1984).
[7]B. W. Keelan and A. H. Zewail, J. Chem. Phys. **82**, 3011 (1985).
[8]T. S. Zwier, E. Carrasquillo M., and D. E. Levy, J. Chem. Phys. **78**, 5493 (1983); C. A. Taatjes, W. B. Bosma, and T. S. Zwier, Chem. Phys. Lett. **128**, 127 (1986).
[9]A. Amirav and J. Jortner, Chem. Phys. Lett. **95**, 295 (1983).
[10]P. M. Felker and A. H. Zewail, J. Phys. Chem. **88**, 6106 (1984); P. M. Felker, W. R. Lambert, and A. H. Zewail, J. Chem. Phys. **82**, 3003 (1985).
[11]W. R. Lambert, P. M. Felker, and A. H. Zewail, J. Chem. Phys. **75**, 5958 (1981); **81**, 2209, 2217 (1984); P. M. Felker and A. H. Zewail, *ibid.* **82**, 2975, 2994 (1985).
[12]D. K. Negus, D. S. Green, and R. M. Hochstrasser, Chem. Phys. Lett. **117**, 409 (1985).
[13]P. R. Bevington, *Data Reduction and Error Analysis for the Physical Sciences* (McGraw–Hill, New York, 1969).
[14]R. H. Dyck and D. S. McClure, J. Chem. Phys. **36**, 2326 (1962).
[15]G. Hohlneicher and B. Dick, J. Photochem. **27**, 215 (1984).
[16]S. Haroche, in *High Resolution Laser Spectroscopy*, edited by K. Shimoda (Springer, New York, 1976), p. 254.
[17]G. Herzberg, *Molecular Spectra and Molecular Structure* (Van Nostrand Reinhold, New York, 1945), Vol. II, p. 48.
[18]M. Traetteberg, E. B. Frantsen, F. C. Mijlhoff, and A. Hoekstra, J. Mol. Struct. **26**, 57 (1975).
[19]A. Warshel, J. Chem. Phys. **62**, 214 (1975).
[20]See Ref. 18 for other studies and a discussion of results.
[21]J. S. Baskin, D. Semmes, and A. H. Zewail, J. Chem. Phys. **85**, 7488 (1986).
[22]Holding A' fixed in the fitting process resulted in a violation of the geometric constraint $A^{-1} > C^{-1} - B^{-1}$. Simulations carried out with A' reduced to meet this constraint are indistinguishable in all important respects from those shown.
[23]While the sum $B' + C'$ is essentially independent of the phenyl twist angle in stilbene, the described analysis of the recurrence form favors an excited state geometry with a center of inversion, as predicted by theory (Ref. 19) but not by electron diffraction studies (Ref. 18). Recent spectroscopic studies indicate a geometry with a center of inversion (Ref. 24).
[24]L. H. Spangler, R. V. Zee, and T. S. Zwier, J. Phys. Chem. (to be published); T Suzuki, N. Mikami, and M. Ito, *ibid.* **90**, 6431 (1986).
[25](a)G. M. Nathanson and G. M. McClelland, J. Chem. Phys. **81**, 629 (1984); (b) A. P. Blokhin and V. A. Tolkachev, Opt. Spectrosc. **51**, 152 (1981).